Stronger Limits on Hypothetical Yukawa Interactions in the 30–8000 nm Range

Y.-J. Chen,[1,2] W. K. Tham,[1] D. E. Krause,[3,4] D. López,[5] E. Fischbach,[4] and R. S. Decca[1,*]
[1]Department of Physics, Indiana University–Purdue University Indianapolis, Indianapolis, Indiana 46202, USA
[2]Section 3, N16 Process Integration Department 1, Taiwan Semiconductor Manufacturing Company, HsinChu 30078, Taiwan
[3]Physics Department, Wabash College, Crawfordsville, Indiana 47933, USA
[4]Department of Physics and Astronomy, Purdue University, West Lafayette, Indiana 47907, USA
[5]Center for Nanoscale Materials, Argonne National Laboratories, Argonne, Illinois 60439, USA
(Received 4 November 2014; revised manuscript received 3 January 2016; published 2 June 2016)

We report the results of new differential force measurements between a test mass and rotating source masses of gold and silicon to search for forces beyond Newtonian gravity at short separations. The technique employed subtracts the otherwise dominant Casimir force at the outset and, when combined with a lock-in amplification technique, leads to a significant improvement (up to a factor of 10^3) over existing limits on the strength (relative to gravity) of a putative force in the 40–8000 nm interaction range.

DOI: 10.1103/PhysRevLett.116.221102

Although the gravitational attraction between two point masses was the first force to be described, it remains, in comparison with other fundamental forces, poorly characterized. Unification theories, such as string theory, which introduce n compact extra spatial dimensions, predict deviations from Newtonian gravity over submillimeter scales [1,2]. Also, many extensions to the standard model predict the existence of new light bosons, the exchange of which would lead to new forces. In both cases, the existence of compact extra dimensions and the exchange of new light bosons, the non-Newtonian interaction between two point masses m_1 and m_2 separated by a distance r can be parametrized as

$$V(r) = -G\frac{m_1 m_2}{r}\alpha e^{-r/\lambda}, \tag{1}$$

where G is the Newtonian gravitational constant, α is the strength of the Yukawa-like correction arising from new physics, and λ is its characteristic range. In the case of compact extra dimensions, λ closely corresponds to the size of the extra dimension. For the exchange of a boson of mass m, $\lambda = \hbar/mc$ [3].

Motivated in part by these considerations a large number of experiments have been conducted to constrain the value of α (see, for example, the reviews [4,5]). While they have been successful in constraining $|\alpha| < 1$ for $\lambda > 50$ μm [6], the limits on α are much less restrictive for $\lambda < 10$ μm. Constraints on α for small values of λ are much more difficult to achieve due to the small effective masses (i.e., mass within a distance $r \sim \lambda$ of the surface) interacting through the Yukawa-like contribution. Compounding the problem at submicron separations, the effects of vacuum fluctuations eventually become dominant after electrostatic contributions have been minimized. Hence, many of the limits in the $\lambda \in [10, 10000]$ nm range have been obtained by subtracting from the measured interaction the calculated contribution from the Casimir force [7–10] which arises from vacuum fluctuations. While useful, this approach has two main drawbacks. (i) The subtracted background is relatively large, and hence small corrections to the background result in large changes in the derived limits. (ii) It is not clear what the appropriate background to subtract is. While some groups use a plasma model for the extrapolation to zero frequency of the dielectric function of the metal, others use a Drude model [11]. The correct approach remains a matter of controversy, and new experiments have been proposed to help resolve this problem [12].

In the absence of electromagnetic contributions, a comparison of the forces exerted on a test mass by materials of different densities leads to constraints on α and λ in Eq. (1). Different materials differ not only in their densities but also in their response to vacuum fluctuations, and hence these effects must be suppressed when searching for the presence of putative new forces at submicron separations. The "isoelectronic" or "Casimir-less" technique introduced in Ref. [13] capitalizes on the fact that the response of a sample to vacuum fluctuations is mainly a surface effect, whereas any new force interacts with a portion within range $\sim\lambda$ of its surface. In the Casimir-less technique, contributions from vacuum fluctuations are suppressed by coating the source mass with a layer of Au having a thickness larger than the plasma wavelength of Au, $\lambda_p = 135$ nm, such that the difference in the Casimir interaction between the underlying structure in the source mass with the test mass is attenuated by a factor larger than 10^6 [13,14]. The Au layer thus serves not only to reduce conventional electrostatic effects as in other experiments but, more significantly, to suppress vacuum fluctuation contributions associated with the composition of the test mass.

While earlier experiments successfully demonstrated the possibility of subtracting the Casimir background, the performance of the technique was limited by two

experimental constrains. (i) To observe a signal at the resonance frequency ω_r of the mechanical oscillator (without anything moving at ω_r) a heterodyne technique was used. The test mass was harmonically positioned over the two sides of the source mass at ω_1, while the separation between the test and source masses was harmonically varied with amplitude δz at $\omega_2 = \omega_r - \omega_1$, effectively reducing the hypothetical Yukawa-like signal by $\delta z/\lambda \sim 0.02$. (ii) The sample was made in such a way that the thicknesses of the two sides of the source mass were unintentionally different. This translated into a $\sim$3 fN systematic signal identified with the distance dependence of the Casimir force. This residual signal yielded the limits obtained in Ref. [13].

In this Letter we report on a new approach to improving the limits in the $\{\lambda, \alpha\}$ phase space. The use of a rotating source mass allowed us to fully utilize the high force sensitivity provided by the large mechanical quality of the microelectromechanical torsional oscillator (MTO) [15]. Furthermore, an implementation of the source mass where there is no correlation between its thickness and its angular position yielded an unprecedented level of subtraction of the background arising from vacuum fluctuations.

A schematic of the experimental setup is shown in Fig. 1. The test mass (a $R = 149.3 \pm 0.2$ μm sapphire sphere covered with a $t_{\mathrm{Cr}} \sim 10$ nm layer of Cr and a $t_{\mathrm{Au}} \sim 250$ nm Au film) was glued close to the edge (at a distance $b = 235 \pm 4$ μm from the axis of rotation) of the 500 μm $\times$ 500 μm plate of the oscillator. Gluing the sphere reduced the MTO's natural frequency of oscillation from $f_0 = 708.23 \pm 0.05$ Hz to $f_r = 307.34 \pm 0.05$ Hz, and it

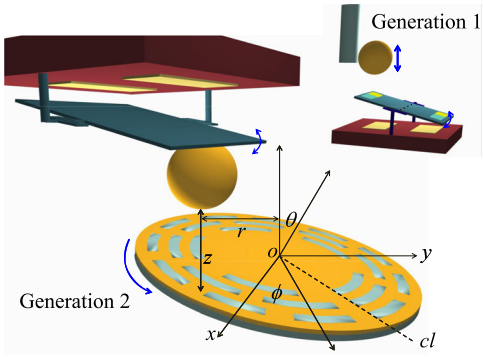

FIG. 1. Schematic of the experimental setup (not drawn to scale). The Au-coated sphere is glued to the oscillator. Three regions with $n = 5, 8, 11$ Au-Si sectors are shown. The actual sample has $n = 50, 75, \ldots, 300$. The $\{x, y\}$ plane defines the plane of rotation of the spindle. cl is the line where all of the different regions with Au-Si sectors coincide. θ is the instantaneous axis of rotation, $\phi = \omega t$ is the angle of rotation. The distance z is measured from the vertex of the spherical test mass to the source mass. r is the distance from the vertex of the test mass to the center of the source mass, o. For clarity, displacements Δr between o and the axis of rotation are not shown. For comparison, a schematic of the setup used in Ref. [13] is shown.

reduced the oscillator's quality factor from $Q \sim 9000$ to $Q \simeq 7200$ for a pressure $P \leq 10^{-5}$ torr. The experiments were performed at $P \simeq 10^{-5}$ torr and the motion of the plate was detected by the change in capacitance between the plate and the underlying electrodes as in Refs. [13,16,17]. Calibration of the MTO was performed by using the electrostatic interaction between the Au-coated test and source masses [16]. The calibration was performed with the source mass stationary, and the distance was monitored and measured using a two-color interferometer (with a sensitivity of 0.2 nm). After performing the calibration, the potential difference between the sphere and the plate was adjusted to minimize the electrostatic interaction. With this MTO, a thermally limited minimum detectable force $F_{\mathrm{min}}(f_r) \sim 6$ fN$/\sqrt{\mathrm{Hz}}$ was calculated when working at resonance at 300 K [18]. Since f_r is a function of separation due to the nonlinear nature of the Casimir interaction, it was continuously monitored.

A five axis stepper-motor-driven positioner and a three axis piezoelectrically driven system were used to bring the test mass in close proximity ($z \in [200, 1000]$ nm) to the source mass. The source mass was fabricated by depositing a $d_{\mathrm{Cr}} = 10$ nm thick layer of Cr on a 1 in. diameter 100 μm thick [100] oriented Si wafer. A $d_{\mathrm{TM}} = 2.10 \pm 0.02$ μm thick layer of Si was deposited on top of the Cr-covered Si wafer. Using conventional photolithography, a photoresist structure consisting of concentric sectors was defined in the Si. The Si not covered by the photoresist was removed down to the Cr layer using CF_4 reactive ion etching. After removing the photoresist, Au was thermally evaporated and the structure mechanically polished to expose the Si sectors. This process defined a structure with a surface consisting of a center circle of Au with a radius $R_1 = 4$ mm, then a 200 μm wide ring with 50 sectors of Au-Si, and a 150 μm wide Au ring. The sequence of 200 μm wide rings with Au-Si sectors and 150 μm wide Au rings was repeated, with the number of Au-Si sectors increasing by 25 for each concentric ring until the last one, with 300 sectors, which was located at $R_{11} = 7.5$ mm. This structure was glued with NOA61 UV curing cement to a BK7 Schott glass flat with the original Si wafer exposed. The wafer was etched away using KOH, and then a $d_{\mathrm{Au}} = 150 \pm 3$ nm layer of Au was deposited by thermal evaporation. The exposed Au surface was characterized by white light interferometry and atomic force microscopy (AFM), which showed an optical quality film with no memory of the underlying structure. The 1024×1024 AFM images obtained over different 10 μm $\times$ 10 μm regions yielded position-independent 60 nm peak-to-peak topographic roughness. Excluding a few isolated spikes $\sim$50 nm tall and about 100 nm across, the sample has a rms roughness of 1.5 nm. The disk was then mounted on an air bearing spindle. It was optically verified that the center of the disk and the axis of rotation of the spindle coincided to better than $\Delta r \sim 10$ μm. The flatness and alignment of the sample

were checked *in situ* using a fiber interferometer (with a response time of 10 ms). It was found that the surface of the sample was perpendicular to the axis of rotation to better than $z_0 = 20$ nm at R_{11} when rotating the disk at $\omega = 2\pi$ rad/s.

The air bearing spindle worked under a constant air flow of several liters per minute. The top of the source mass was at a distance $D = 4$ cm from the air exhaust. To prevent air leaks into the chamber, the spindle was mounted with a circular skirt which rotated with the spindle. The seal between the skirt and the vacuum chamber was provided by high molecular weight oil. Oil contamination inside the chamber was precluded using chilled water refrigeration ($T = 10\,°\mathrm{C}$) on a system of baffles and traps.

With the sphere placed at $R_i + 100\ \mu$m (with n Au-Si sectors), the air bearing spindle was rotated at $\omega_r = 2\pi f_r/n$. In this manner, a force arising from the potential given in Eq. (1) would have manifested itself at f_r, even though there were no parts moving at f_r. The Newtonian gravitational attraction between the sphere and the structured sample yields a force $F_N \sim 10^{-20}$ N, undetectable by our system. Hence, an integration of Eq. (1) over the geometry of the sample is necessary. Disregarding finite size effects across the width of the ring [17], the expected difference when the sphere is over a Au or Si sector is [13,19]

$$\begin{aligned}\Delta F_h(z) &= -4\pi^2 G\alpha\lambda^3 e^{-z/\lambda} R K_t K_s,\\ K_t &= [\rho_{\mathrm{Au}} - (\rho_{\mathrm{Au}} - \rho_{\mathrm{Cr}})e^{-t_{\mathrm{Au}}/\lambda}\\ &\quad -(\rho_{\mathrm{Cr}} - \rho_{\mathrm{S}})e^{-(t_{\mathrm{Au}}+t_{\mathrm{Cr}})/\lambda}],\\ K_s &= [(\rho_{\mathrm{Au}} - \rho_{\mathrm{Si}})e^{-(d_{\mathrm{Au}}+d_{\mathrm{Cr}})/\lambda}(1 - e^{-d_{\mathrm{TM}}/\lambda})], \quad (2)\end{aligned}$$

where K_t (K_s) is a term associated only with the layered structure of the test (source) mass, ρ_{S}, ρ_{Cr}, ρ_{Au}, and ρ_{Si} are the sapphire, Cr, Au, and Si densities, respectively.

The setup is optimized to select the first harmonic of the force associated with the angular distribution of the sample. Other harmonics and all forces with different angular dependences are outside of the resonance peak of the MTO and consequently are "filtered" by the sharp $\Delta f \simeq 40$ mHz resonance peak of the oscillator.

Results obtained by doing the experiment over the $n = 300$ ring are shown in Fig. 2. These results were obtained by using a lock-in detection technique at f_r. A mark on the outside of the source mass coincident with the cl line in Fig. 1 was used to define the origin of the phase. Many features are worth noting. (i) Increasing the integration time τ decreases the random noise of the measured force, as expected. (ii) At separations $z \leq 300$ nm, the statistical noise is larger than the minimum detectable force. This happens in a region where the Casimir force is large. At larger separations, the statistical noise is close to the minimum detectable force. It was also observed that this noise was independent of the angular frequency of the

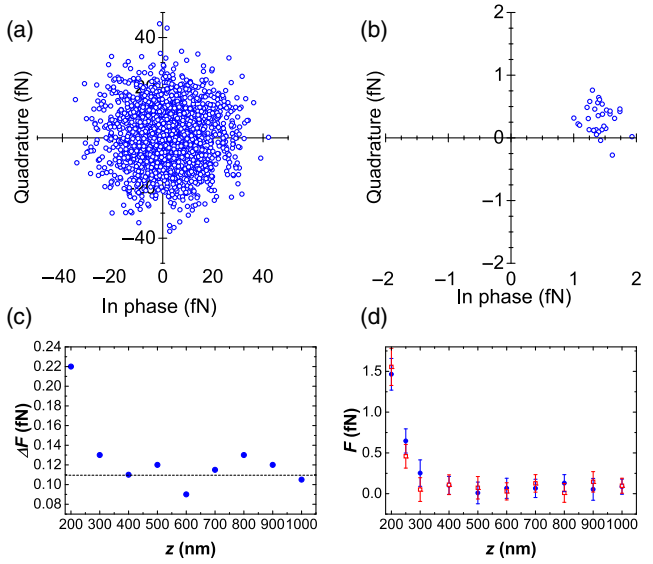

FIG. 2. (a) Lock-in amplified detection of the signal with an integration time $\tau = 1$ s at a separation $z = 200$ nm. (b) Same as in (a) for $\tau = 3000$ s. (c) Standard deviation for 15 different realizations of the experiment, with $\tau = 3000$ s as a function of separation. The horizontal dashed line is the statistical noise in the amplitude of the oscillator at $T = 293$ K (which was also measured over $\tau = 12000$ s at $z = 3\ \mu$m). (d) Measured interaction as a function of separation. The two data sets were obtained on top of the region with $n = 300$ (filled circle) and over a section of the sample without Si at a radius $r = 8$ mm (square). The error bars represent the standard deviation for ten repetitions with $\tau = 3000$ s.

disk (for $\omega/2\pi \in [0.2, 20]$ Hz). (iii) There is a separation-dependent net force measured which is practically independent of the radial position of the sphere over the rotating disk. This signal increases proportionally to ω as the disk is rotated at higher subharmonics of $\omega_r = 2\pi f_r$.

Point (iii) indicates an incomplete subtraction of background forces. Kelvin probe force microscopy was performed in the sample over different $5 \times 5\ \mu\mathrm{m}^2$ regions. This contribution is not of electrostatic origin. It was observed that the main potential islands had a characteristic size $\ell \sim 200$ nm, with $V_{\mathrm{rms}} < 5$ mV. Since the experimental system provides a sharp filtering of the signal at ω_r, this implies that the electrostatic contribution to the signal at ω_r would be undetectable, $\Delta F_{\mathrm{el}}(z) \leq 10^{-17}$ N [20]. Furthermore, if detected, the electrostatic signal would have a radial dependence when the disk is rotated at constant frequency [20], which was not observed.

Variations in the separation between test and source masses could yield the observed background through the separation dependence of the Casimir force $F_C(z) \propto z^{-\alpha}$ [11]. $F_C(200\ \mathrm{nm}) = 34$ pN and $\alpha = 2.78$ were experimentally determined in the actual configuration. The observed signal at $\omega_r = n\omega$ must appear through $z(t)$.

The observed signals are consistent with the axis of rotation of the spindle having both an impulselike $\Delta\theta_1$

once-per-revolution and a random wobbling. The impulselike wobble has been identified by analyzing its frequency dependence. Varying the frequency of the spindle, the harmonic components of the signal observed at ω_r are consistent with a once-per-revolution impulselike signal. The random wobbling is observed to have white-noise characteristics, $\langle\theta_2(\tau)\theta_2(0)\rangle = \Theta^2\delta(\tau)$, where Θ is a constant, in the range of frequencies investigated, between 0.1 and 20 Hz. This random noise increases the minimum detectable force from ~6 to ~12 fN/$\sqrt{\text{Hz}}$ at $z = 200$ nm. Associated with any $\Delta\theta$, there is a change in separation $\delta z \sim D\delta\theta$ between the sphere and the rotating sample, which induces a change in the Casimir force. Since, in our experiment, $D \sim 4$ cm, it follows that $\Theta \sim 5 \times 10^{-10}$ rad and $\Delta\theta_1 \leq 10^{-7}$ rad. Neither of these angular deviations can currently be measured directly.

The lack of parallelism between the normal to the disk and the rotational axis leads to the time-varying separation $z(t) = z_s + z_0\cos(\omega t)$. Its contribution ΔF_{par} at ω_r enters through the nonlinear dependence of the Casimir force on the separation. A Taylor's expansion of $F_C(z) \propto z^{-\alpha}$ shows that the contribution at ω_r is attenuated by $\sim(z/z_0)^n$, making it unobservable for all n's in our setup. This is also the case for precession of the spindle. Similarly, the lack of flatness of the sample generates the angular-position-dependent separation $z(\phi)$, which was measured using white light interferometry (see the inset in Fig. 3). Inserting these data into $F_C(z)$ yields a contribution $\Delta F_{\text{top}} < 0.05$ fN.

The effect of the once-per-revolution $\Delta\theta_1$ was minimized in the following way: $\Delta\theta_1$ happens at a characteristic ϕ_o. As the disk is positioned for the first time on the spindle, there is an unknown angle ϕ_x between the line cl and the line defined by ϕ_o. When the sphere is positioned over a region with only Au in the source mass, a signal with a nonzero phase is detected (recall that the zero phase is defined at cl). The sample is then very carefully repositioned over the disk until the phase of the detected signal is zero. In this situation, $\phi_x = 0$ is assumed.

An approach where the zero of the phase is redefined could also be used [21]; however, the method of repositioning the sample is superior to redefining the zero of the phase. While it is expected that the signal described by Eq. (2) is in quadrature (i.e., it should be an odd signal with respect to ϕ), in principle, it is not known whether the model is correct. The data shown in Fig. 3 were obtained in this manner. Furthermore, the same component of the signal in phase was measured with the sphere placed at any radii. It was determined that the hypothetical force (in quadrature) is consistent with zero within the experimental error for any radii R_n.

The Δr shift between the axis of rotation and the center of the source mass would also yield a signal at ω if ΔF_h were observable, although it would be attenuated by $R_i/\Delta r$ at ω_r. Similarly, finite size effects as the Au-Si interface of the source mass moves under the test mass are negligible at ω_r when compared with the statistical errors.

While the relevant error is ΔF_{rand}, the overall error was obtained as an addition of the random and systematic errors $\Delta F = \Delta F_{\text{rand}} + \Delta F_{\text{syst}}$. The individual systematic errors described in this Letter were considered to be independent to obtain ΔF_{syst}. $F(z)$ in Fig. 3 associated with the hypothetical force is consistent with zero and was used to establish new limits in $\{\lambda, \alpha\}$ space at the 95% confidence level. The envelope of the curves where the first harmonic of $F_h(z)$ is compared with $\max\{|F(z) + 2\Delta F(z)|, |F(z) - 2\Delta F(z)|\}$ is shown in Fig. 4. The new limits obtained with the introduced

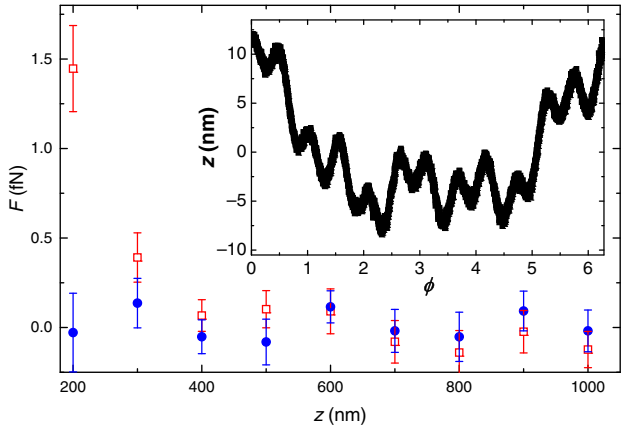

FIG. 3. Measured interaction as a function of separation obtained on top of the region with $n = 300$. (filled circle) quadrature signal; (square) in phase signal (see the text). Errors represent the standard deviation for ten repetitions with $\tau = 3000$ s. (Inset) The sample's topography, $z(\phi)$ over the R_{11} circle, obtained by white light interferometry.

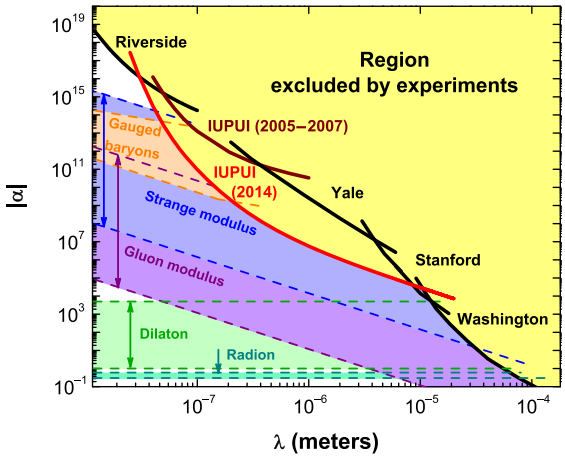

FIG. 4. Values in the λ, α phase space excluded by experiments. The red curve represents the limits obtained in this work. Previous limits from Riverside [22], IUPUI [9,13], Yale [23], Stanford [24], Washington [25], and theoretical predictions [1,2,26–28] are also shown.

Casimir-less measurement technique represent a significant improvement over previous experiments: new boundaries have been established in a spatial range covering more than 3 orders of magnitude ($\lambda \in [30, 8000]$ nm), with improvements as large as 10^3 in Yukawa-like corrections to Newtonian gravity at $\lambda = 300$ nm.

This work was performed, in part, at the Center for Nanoscale Materials, a U.S. Department of Energy, Office of Science, Office of Basic Energy Sciences User Facility under Contract No. DE-AC02-06CH11357. R. S. D. acknowledges support from the National Science Foundation through Grant No. PHY-0701636 and from Los Alamos National Laboratory through Contract No. 49423-001-07. R. S. D. is also indebted to the IUPUI Nanoscale Imaging Center, the IUPUI Integrated Nanosystems Development Institute, and the Indiana University Center for Space Symmetries for their financial and technical support. The work of E. F. was supported in part by U.S. Department of Energy Contract No. DE-AC02-76ER071428.

*rdecca@iupui.edu

[1] N. Arkani-Hamed, S. Dimopoulos, and G. Dvali, Phys. Lett. B **429**, 263 (1998); Phys. Rev. D **59**, 086004 (1999).
[2] E. G. Adelberger, B. R. Heckel, and A. E. Nelson, Annu. Rev. Nucl. Part. Sci. **53**, 77 (2003).
[3] E. Fischbach and C. L. Talmadge, *The Search for Non-Newtonian Gravity* (Springer, New York, 1999).
[4] E. G. Adelberger, J. H. Gundlach, B. R. Heckel, S. Hoedl, and S. Schlamminger, Prog. Part. Nucl. Phys. **62**, 102 (2009).
[5] J. Murata and S. Tanaka, Classical Quantum Gravity **32**, 033001 (2015).
[6] D. J. Kapner, T. S. Cook, E. G. Adelberger, J. H. Gundlach, B. R. Heckel, C. D. Hoyle, and H. E Swanson, Phys. Rev. Lett. **98**, 021101 (2007).
[7] T. Ederth, Phys. Rev. A **62**, 062104 (2000); V. M. Mostepanenko and M. Novello, Phys. Rev. D **63**, 115003 (2001).
[8] B. W. Harris, F. Chen, and U. Mohideen, Phys. Rev. A **62**, 052109 (2000).
[9] R. S. Decca, D. López, E. Fischbach, G. L. Klimchitskaya, D. E. Krause, and V. M. Mostepanenko, Eur. Phys. J. C **51**, 963 (2007); Phys. Rev. D **75**, 077101 (2007).
[10] A. O. Sushkov, W. J. Kim, D. A. R. Dalvit, and S. K. Lamoreaux, Nat. Phys. **7**, 230 (2011).
[11] See, for example, G. L. Klimchitskaya, U. Mohideen, and V. M. Mostepanenko, Rev. Mod. Phys. **81**, 1827 (2009).
[12] G. Bimonte, Phys. Rev. Lett. **112**, 240401 (2014).
[13] R. S. Decca, D. López, H. B. Chan, E. Fischbach, D. E. Krause, and C. R. Jamell, Phys. Rev. Lett. **94**, 240401 (2005).
[14] R. Matloob and H. Falinejad, Phys. Rev. A **64**, 042102 (2001); while the model presented is not exact, it is accurate to within a few percent, sufficient for the purposes of this work.
[15] D. López, R. S. Decca, E. Fischbach, and D. E. Krause, Bell Labs Techn. J. **10**, 61 (2005).
[16] R. S. Decca and D. López, Int. J. Mod. Phys. A **24**, 1748 (2009).
[17] C. R. Jamell and R. S. Decca, Int. J. Mod. Phys. A **26**, 3742 (2011).
[18] Away from resonance, the electronic background imposes a constraint on the minimum detectable force. In our case, it is ~0.5 pN.
[19] R. S. Decca, E. Fischbach, G. L. Klimchitskaya, D. E. Krause, D. López, and V. M. Mostepanenko, Phys. Rev. D **79**, 124021 (2009).
[20] R. O. Behunin, D. A. R. Dalvit, R. S. Decca, and C. C. Speake, Phys. Rev. D **89**, 051301(R) (2014).
[21] It was verified that the same results were obtained by a simple change of phase in the lock-in detection scheme.
[22] U. Mohideen and A. Roy, Phys. Rev. Lett. **81**, 4549 (1998); G. L. Klimchitskaya, A. Roy, U. Mohideen, and V. M. Mostepanenko, Phys. Rev. A **60**, 3487 (1999); A. Roy and U. Mohideen, Phys. Rev. Lett. **82**, 4380 (1999); B. W. Harris, F. Chen, and U. Mohideen, Phys. Rev. A **62**, 052109 (2000).
[23] A. O. Sushkov, W. J. Kim, D. A. R. Dalvit, and S. K. Lamoreaux, Phys. Rev. Lett. **107**, 171101 (2011).
[24] J. Chiaverini, S. J. Smullin, A. A. Geraci, D. M. Weld, and A. Kapitulnik, Phys. Rev. Lett. **90**, 151101 (2003); A. A. Geraci, S. J. Smullin, D. M. Weld, J. Chiaverini, and A. Kapitulnik, Phys. Rev. D **78**, 022002 (2008).
[25] D. J. Kapner, T. S. Cook, E. G. Adelberger, J. H. Gundlach, B. R. Heckel, C. D. Hoyle, and H. E. Swanson, Phys. Rev. Lett. **98**, 021101 (2007).
[26] D. B. Kaplan and M. B. Wise, J. High Energy Phys. 08 (2000) 037.
[27] I. Antoniadis, K. Benakli, A. Laugier, and T. Maillard, Nucl. Phys. **B662**, 40 (2003).
[28] S.-Q. Yang, B.-F. Zhan, Q.-L. Wang, C.-G. Shao, L.-C. Tu, W.-H. Tan, and J. Luo, Phys. Rev. Lett. **108**, 081101 (2012).